

EFFICIENCY IN COLLISIONLESS GROWTH OF PLANETESIMALS

ANDREW SHANNON^{1,3}, YANQIN WU¹ & YORAM LITHWICK²

¹Department of Astronomy and Astrophysics, University of Toronto, Toronto, ON M5S 3H4, Canada;

²Department of Physics and Astronomy, Northwestern University, Evanston, IL 60208 and Center for Interdisciplinary Exploration and Research in Astrophysics (CIERA) and

³Institute of Astronomy, University of Cambridge, Madingley Road, Cambridge CB3 0HA, UK

Draft version March 19, 2013

ABSTRACT

We study the efficiency of growing large bodies, starting from a sea of equal-sized planetesimal seeds. This is likely one of the earlier steps of planet formation and is related to the origin of the asteroid belt, the Kuiper belt and extra-solar debris disks. Here we study the case that the seeds do not collide frequently enough for dynamical cooling to be important (the collisionless limit), using a newly constructed conglomeration code, and by carefully comparing numerical results with analytical scalings. We find that large bodies grow primarily by accreting small seeds (and not by accreting each other). As the velocity dispersion of the small bodies (u) is increasingly excited by the growing big bodies, growth passes from the well-known run-away stage (when u is higher than the big bodies' hill velocity) to the newly discovered trans-hill stage (when u and big bodies both grow, but u remains at the big bodies' hill velocity). We find, concurring with analytical understandings developed in Lithwick (2013), as well as previous numerical studies, that a size spectrum $dn/dR \propto R^{-4}$ results, and the formation efficiency, defined as mass fraction in bodies much greater than the seed sizes, is \sim a few $\times R_{\odot}/a$, or $\sim 10^{-3}$ at the distance of the Kuiper belt. This extreme inefficiency argues against the collisionless limit for the formation of the Kuiper belt and extra-solar debris disks. To conglomerate large bodies in those regions, the initial planetesimals may have to be small and highly collisional.

1. INTRODUCTION

Large solid bodies, ranging in size from less than a kilometer to thousands of km roam in the outskirts of both the solar and many extrasolar systems. In the case of the solar system, Pluto, Sedna and other large Kuiper belt objects are directly detected (Slipher & Tombaugh 1930; Jewitt & Luu 1993; Brown et al. 2005; Schlichting et al. 2009); and in the case of extrasolar ones, these bodies are inferred from the dust grains that are produced during their mutual collisions. Even a small amount of dust can intercept enough star light to become detectable as debris disks (Aumann et al. 1984; Wyatt 2008). Surprisingly, $\sim 20\%$ of solar-type stars, even at an age similar to the Sun, harbor dust disks that are brighter than ours by more than three orders of magnitude (Meyer et al. 2007).

How do these large bodies form? Are they an intermediate step in the formation route for planets? Why are they not incorporated into Earth or even Neptune-like planets? Why are many exo-debris disks so bright yet ours so anemic? These are the questions we set out to answer.

The conventional picture for the formation of our own Kuiper belt (Kenyon & Luu 1998; Ormel et al. 2010; Schlichting & Sari 2011, hereafter SS11) postulates that it started from ~ 10 Earth masses of primordial rock and ice (\sim solid mass in the Minimum Mass Solar Nebulae), and only a fraction $\epsilon \sim 10^{-3}$ of this mass conglomerated into the large Kuiper belt bodies we see today. The rest was somehow removed. This extremely low efficiency occurs because, theorists argue, as bodies like Pluto grow, they stir the orderly orbital motion of the seed material to such an extent that the latter can no longer be accreted

quickly into large bodies: Plutos starve themselves.

However, there are four serious issues with this paradigm. First, exo-debris disks are too bright. The total mass contained in their large objects must be ~ 1000 times that in our own system (Shannon & Wu 2011). According to the conventional picture of Kuiper belt formation, this would have required $\sim 10^4$ Earth masses of primordial solids, some 1000 times more than the value expected in a minimum mass solar nebula. Second, a $\sim 10M_{\oplus}$ disk of kilometer bodies would have disrupted the long period Kuiper belt binaries, which are observed in abundance (Parker et al. 2011; Parker & Kavelaars 2012). Third, the removal of most of the primordial solids, by first grinding them down to dust grains and then blowing them out using radiation pressure, may not work on theoretical grounds (Lithwick et al., in preparation). Fourth, the low formation efficiency is incompatible with some theories of Neptune migration (Thommes et al. 1999; Gomes et al. 2004) where a vast majority of the Pluto-like large bodies, if formed prior to Neptune's migration, were stipulated to have been scattered away by giant planets (Stern 1991; Levison et al. 2008).

We explore a different route, stimulated by the theoretical proposal of Goldreich et al. (2004b, hereafter GLS). Different from all previous works (e.g., Safronov 1969; Greenberg et al. 1978; Wetherill & Stewart 1989; Kenyon & Luu 1998; Kenyon & Bromley 2008; Ormel et al. 2010; Schlichting & Sari 2011), we model the planetesimals as being so small that their mutual collisions are dynamically important. In this picture, as seed materials are stirred up their destructive collisions grind them down to smaller debris. Smaller seeds collide

much more frequently than larger ones and their relative velocities remain low. This collisional cooling guarantees efficient accretion by large bodies, until almost all mass has been converted to large bodies. Such a picture will allow the *in situ* formation of the cold classical Kuiper belt (Shannon et al. 2013a), and explain the high mass in bright exo-debris disks (Shannon et al. 2013b).

But for the current publication, we restrict ourselves to the conventional case of no collisional cooling. There are three purposes to this paper. One is to document our coagulation code and certify its various components against analytical expectations (§2). This code contains collisional break-down and cooling, but these two effects are unimportant here since we adopt large initial sizes for the planetesimals. Second, our results demonstrate clearly (§3) that, in the case of collisionless growth, the formation efficiency is limited to $\epsilon \sim \text{a few} \times \alpha$ where $\alpha = R_{\odot}/a$, i.e., α is the angle subtended by the Solar disk at distance a . In the Kuiper belt region, $\alpha \sim 10^{-4}$. Hence only $\epsilon \sim 10^{-3}$ of the initial mass could have been incorporated into large bodies that one observes there today (if growth was nearly collisionless). Equivalently, to form these bodies the initial mass in planetesimals would have had to be $\sim 10M_{\oplus}$, similar to that expected in a MMSN disk extrapolated to the Kuiper belt distance, (Weidenschilling 1977; Hayashi 1981)). Lastly, we compare results from our code against previous work (§4). In particular, SS11 have recently proposed a simple explanation for the size distribution of Kuiper belt bodies, in the case of collisionless conglomeration. We examine their claim critically.

This paper should be considered a numerical companion to the recent work by Lithwick (2013) where a conglomeration phase called ‘trans-hill growth’ is first discussed. That paper, largely analytical, arrives at similar conclusions as reached here.

2. THE CONGLOMERATION CODE: COMPONENT TESTING

We adopt a particle-in-a-box approach (Safronov 1969) to study the interactions of planetesimals and their growth. The range of body sizes we track runs from $\sim \text{km}$ to $\sim 10^3 \text{ km}$.¹ Since the total number of particles active in our simulations can exceed 10^{15} , and we typically integrate the system for up to 10^6 dynamical times, we adopt by necessity a statistical approach where particles with similar properties (mass, eccentricity, inclination, semi-major axis) are grouped into the same bin. We do not yet have the capability of coupling N-body integrators with the statistical code, as was done by Bromley & Kenyon (2006); Kenyon & Bromley (2008); Glaschke (2006). As such, we fail to capture the evolution correctly at late times, when only a few large bodies dominate the evolution.

2.1. Particles and Bins

A total of six parameters are needed to specify an orbit. We choose the semi-major axis a , the eccentricity e , the inclination i , the argument of periape ω , the longitude of the ascending node Ω , and the mean anomaly M . Together with mass, each particle should be described by

¹ This is expanded in our next work when we consider grains as small as $\sim \mu\text{m}$.

seven parameters. This is computationally prohibitive and approximations are in order. In the following we explain the simplifying assumptions we make in this code.

We adopt a single-value of semi-major axis ($a = 45\text{AU}$) for all particles, spread to a width $\Delta a \sim 0.13a \sim 6\text{AU}$. Our single zone approach limits us to study systems where the eccentricities are small ($e < \Delta a/a$). The particles are assumed to be distributed uniformly in ω , Ω , and M . We set $i = 0.5e$, as is approximately true if random energy is equipartitioned in each dimension (Hornung et al. 1985). So velocity anisotropy, important when particles are very cold (Ida & Makino 1992; Rafikov 2003), is not properly treated here.

These simplifications allow us to describe particles only by their masses and eccentricities. We track particle flow across both the mass bins and the eccentricity bins, as is done in Krivov et al. (2005). This differs from the approach of, e.g., Kenyon & Luu (1998), where particles carry with them floating mass values, i.e., particles of a given mass have a single eccentricity. The eccentricity bins have values from $e = 10^{-7}$ to $e = 1$ and are equally spaced logarithmically with four bins per decade. The mass bins are also equi-spaced in logarithmic space, with six bins per decade of mass (i.e., $\Delta m \approx 1.47m$). Particles of all masses are assigned the same bulk density, $\rho = 1.5\text{g/cm}^3$.

The dispersion velocity of a particle is (Wetherill & Stewart 1993),

$$v = v_{\text{kep}} \sqrt{\frac{5}{8}e^2 + \frac{1}{2}i^2} \quad (1)$$

where $v_{\text{kep}} = \Omega a$ with Ω being the orbital angular frequency.

Processes detailed in the following section drive mass and eccentricity evolution and we use a second-order Runge-Kutta integrator to advance the simulation in time. There are two subtleties in the actual implementation. First, when the outcome of an interaction results in a new mass/eccentricity that falls in between two adjacent bins, we split the particles into the two bins conserving total mass and mass-weighted eccentricity (in the case of eccentricity), and total mass and total number (in the case of mass). Moreover, our integration has a fixed time step, typically set to be 100 years. In the case where dynamical evolution leads to undershooting (negative number of particles) in a bin at the end of a timestep, we reduce the strength of the dynamical interaction such that the bin empties to zero. This is necessary when bodies are strongly affected by processes like viscous stirring and collisional cooling.

2.2. Dynamical Friction & Viscous Stirring

Mutual gravitational interactions lead towards equipartition of random kinetic energies between bodies. This is called dynamical friction (Chandrasekhar 1943). Additionally, in a keplerian disk, gravitational interactions between bodies converts their orbital energy into random kinetic energy. This is called viscous stirring (Safronov 1969).

To model dynamical friction and viscous stirring, we adopt the prescription of Ohtsuki et al. (2002), who provide semi-analytic formulae for the rates at which eccentricity and inclination evolve through gravitational scat-

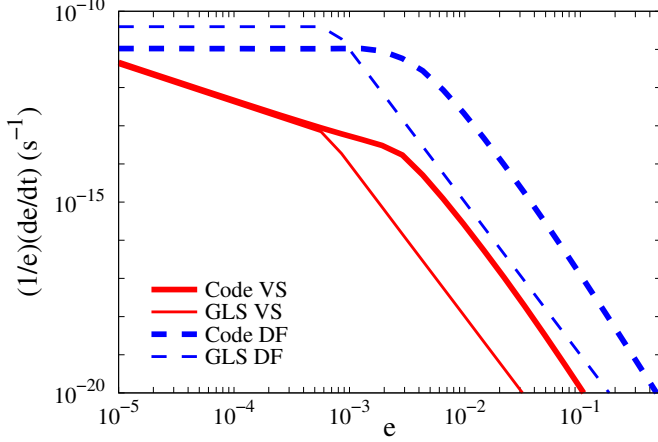


FIG. 1.— The absolute rates of viscous stirring (VS, red solid lines) and dynamical friction (DF, negative in sign and only acting on big bodies, blue dashed lines) used in our code (thick lines), as compared to the order-of-magnitude estimates (thin lines) of GLS, plotted here as functions of eccentricity (e). These rates are for a population of 1000 km big bodies interacting with a population of small bodies, with equal surface densities, $\Sigma = \sigma \sim 0.1\text{g/cm}^3$, and equal dispersion velocities, $u = v = eV_{\text{kep}}$, situated at 45 AU. The bend around $e \sim 10^{-3}$ (Hill velocity of the 1000km bodies) occurs when the velocity dispersion transitions from sub-hill to super-hill. If one substitutes $2.5v_H$ into the GLS expressions whenever v_H appears, as is suggested by N-body experiments (Nishida 1983; Greenberg et al. 1991), the agreements between the two sets of curves will be much closer.

terings, calibrated by N-body simulations. But when the mutual velocity of two bodies are below their mutual Hill velocity (sub-hill), we adopt instead the viscous heating prescription in eq. (13) of Collins et al. (2007), calibrated by the numerical simulations of Collins & Sari (2006).

GLS give explicit formula for the rate of viscous stirring and dynamical friction, depending on whether the velocities are sub- or super-hill (also called shear- or dispersion-dominated). They consider two groups of particles, smaller bodies with size s , surface density σ and velocity dispersion u , and large bodies with radius R , surface density Σ and velocity dispersion v . The two most relevant expressions are viscous stirring of small bodies by the big ones, and dynamical friction of the big bodies by the small bodies. Assuming $u > v$, these are

$$\left. \frac{1}{u} \frac{du}{dt} \right|_{vs} \sim \frac{\Sigma \Omega}{\rho R} \alpha^{-2} \begin{cases} \left(\frac{v_H}{u} \right)^4 & u > v_H, \\ \left(\frac{v_H}{u} \right) & u < v_H \end{cases} \quad (2)$$

$$\left. \frac{1}{v} \frac{dv}{dt} \right|_{df} \sim -\frac{\sigma \Omega}{\rho R} \alpha^{-2} \begin{cases} \left(\frac{v_H}{u} \right)^4 & u > v_H, \\ 1 & u < v_H \end{cases} \quad (3)$$

Viscous stirring of large bodies by themselves can be found by substituting v for u in equation 2. As Fig. 1 shows, our adopted prescriptions agree with the above estimates well, when v_H in the above expressions are sub-

stituted by $2.5v_H$. Here, v_H is the Hill velocity of large bodies,

$$v_H = v_{\text{kep}} \left(\frac{M_{\text{big}}}{3M_{\odot}} \right)^{1/3} \approx 3^{-1/3} \alpha^{-1} \Omega R. \quad (4)$$

The big body mass $M_{\text{big}} = 4\pi/3 \rho R^3$ with ρ being the bulk density. We set ρ to be the mean density of the Sun, and use α to denote the angular size of the Sun, viewed by the bodies, $\alpha = R_{\odot}/a$. For the Kuiper belt, $\alpha \sim 10^{-4}$.

2.3. Collisions: cooling and cascade

Our conglomeration code includes the collisional process. Although not used in this collisionless study, it is essential for our follow-up studies of collisional growth. We document it here for completeness.

In the particle-in-box method, the frequency of collision for a particle is $f_c = n\pi b^2 v$. Here, n is the number density of other particles, πb^2 the cross section for collision, and v the relative velocity. The relative velocity between two particles is simply set to be $v = \sqrt{v_1^2 + v_2^2}$ where v_i is as defined in equation (1).

Under our assumption of evenly distributed orbital angles, particles with eccentricity e occupy a torus in space that has a volume (see, e.g. Krivov et al. 2005),

$$V(e) = \frac{4\pi}{3} a^3 \left[(1+e)^3 - (1-e)^3 \right] \sin i. \quad (5)$$

Their number density is then obtained by $n = N/V$ where N is the particle number. Between two groups of particles with different e 's (e_1, e_2 , but the same a), their overlapping volume is determined by the group with the smaller e (let it be e_1), and the collision frequency is reduced by a ratio of $V(e_1)/V(e_2)$ to take account of the reduced residence time group 2 particles spend inside $V(e_1)$.

We adopt a three-piece form (Greenberg et al. 1991, GLS) for the cross-section for collision between particles of size s_1 and s_2 ,

$$\pi b^2 = \begin{cases} \pi (s_1 + s_2)^2 \left(1 + \frac{v_{\text{esc}}^2}{v^2} \right) & v_H < v, \\ \pi (s_1 + s_2)^2 \left(\sqrt{6} \alpha^{-\frac{1}{2}} \frac{v_H}{v} \right) & \alpha^{\frac{1}{2}} v_H < v < v_H, \\ \pi (s_1 + s_2)^2 \left(\sqrt{6} \alpha^{-\frac{3}{2}} \right) & v < \alpha^{\frac{1}{2}} v_H. \end{cases} \quad (6)$$

We follow GLS and name them *super-hill*, *sub-hill*, and *super-thin* cases. The last case occurs when the velocity dispersion is so small the particles can be regarded as infinitely thin in the vertical direction. These expressions apply when the velocity dispersion is isotropic ($e \sim i$).

The outcome of collisions is modelled as changes in mass and eccentricity. For the eccentricity evolution, we set the orbits of the post-collision particles to be that for their center of mass, independent of the outcome of the collision. For head-on collisions, this corresponds to setting the coefficient of restitution to zero. Let the two bodies have initially masses m_1, m_2 ($m_c = m_1 + m_2$), orbital velocities v_1, v_2 , the constraints of mass and momentum conservation lead to the following expressions for the new orbital elements, (a_f, e_f) (Krivov et al.

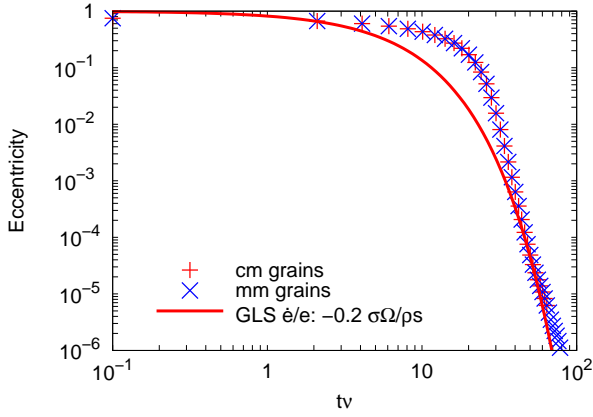


FIG. 2.—: Collisional cooling, in our code (crosses) and from analytical estimate (solid curve). The eccentricity of particles are plotted as functions of rescaled time, tv , where ν is the collisional frequency (eq. 8). Different symbols are for when $s = 1$ cm and when $s = 1$ mm. Numerical cooling rates agree with analytical estimates, as long as the latter rates are decreased by a factor of 5.

2005):

$$\frac{m_c}{2a_f} = \frac{m_1}{m_c} \frac{m_1}{2a_1} + \frac{m_2}{m_c} \frac{m_2}{2a_2} - \frac{m_1 m_2}{m_c} \left(\frac{\mathbf{v}_1 \cdot \mathbf{v}_2}{GM_\odot} - \frac{2}{r} \right),$$

$$m_c a_f \sqrt{1 - e_f^2} = m_1 a_1 \sqrt{1 - e_1^2} + m_2 a_2 \sqrt{1 - e_2^2}, \quad (7)$$

where r is the position of the collision. In our single-zone calculation, we reset a_f to a after applying the above equations. In addition, we evaluate the $\mathbf{v}_1 \cdot \mathbf{v}_2$ term by taking appropriate orbital averaging of the two orbits.

An order-of-magnitude estimate for the rate of collisional cooling among small bodies is (GLS)

$$\frac{1}{u} \frac{du}{dt} = -\frac{\sigma \Omega}{\rho s} = -\nu, \quad (8)$$

where ν is the collisional frequency. We confirm that our collisional code reproduces this scaling (Fig. 2), albeit with a constant factor of ~ 5 offset.

In terms of mass evolution, collisions can lead to catastrophic destruction, (inelastic) rebound, or conglomeration. Catastrophic collision is defined where the primary body loses $\geq 50\%$ of its mass. We specify this to happen if the specific kinetic energy in the impact, $\frac{1}{2} \frac{m_1 m_2}{(m_1 + m_2)^2} v^2$, exceeds the disruption threshold (Stewart & Leinhardt 2009),

$$Q^* \approx 500 (s_1^3 + s_2^3)^{-1/9} v^{0.8} + 10^{-4} (s_1^3 + s_2^3)^{0.4} v^{0.8}, \quad (9)$$

with all numbers in cgs units. This is the scaling for weak aggregates, and may be appropriate for Kuiper belt bodies. For km-sized bodies, $Q^* \sim 150 (v/1 \text{ cm s}^{-1})^{0.8} \text{ erg g}^{-1}$. This corresponds to a disruption velocity of $v \sim 100 \text{ cm/s}$, or $e \approx 10^{-3}$ at 40 AU.

When bodies of size s_1 are catastrophically disrupted, we re-distribute their masses to smaller size bins with a number distribution that is power-law in size, $dn/ds \propto$

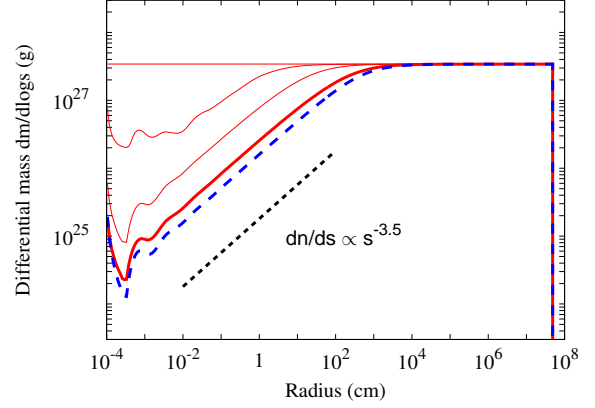


FIG. 3.—: Evolution of the differential mass distribution during a collisional cascade, plotted at $t = 0, 10^4, 10^5, 10^6$ yrs (red curves). Material strength is taken to be constant. As a result, one expects that bodies in collisional equilibrium satisfy $dn/ds \propto s^{-3.5}$ (dotted line). In this simulation, initial surface density $\sigma = 0.1 \text{ g/cm}^2$, and mass of the catastrophically disrupted bodies are distributed to smaller sizes as $dn/ds \propto s^{-4}$. The final size spectrum is insensitive to this debris redistribution: the blue dashed curve shows the size distribution at 10^6 yrs if the redistribution instead follows $dn/ds \propto s^{-2}$. We assume all particles smaller than $1 \mu\text{m}$ are instantly blown away by radiation pressure, which leads to the wavy pattern near the cut-off size, as described in Thébault et al. (2003).

$s^{q'}$ for $s < s_1$. We typically choose $q' = -3.5$. This distribution results in most of the mass ending up in the largest fragments. And Fig. 3 shows that results do not vary when we vary the value of q' from -2 to -4 . Furthermore, to imitate the effect of radiative pressure, we remove all mass in size bins below our minimum size (at one micron). In the future, it may be useful to implement the dependence of the largest fragment mass on the impact energy (Stewart & Leinhardt 2009).

To verify the collisional mass evolution, we test our code against the standard case of collisional equilibrium for which an analytical solution is known. For a material strength $Q^* \propto s^p$, the collisional cascade will carry a constant mass flux downward in particle size and build up an equilibrium size distribution of (Dohnanyi 1969; Durda & Dermott 1997),

$$\frac{dn}{ds} \propto s^{-q} \quad (10)$$

with $q = (21 + p)/(6 + p)$. The well-known Dohnanyi law is the special case with $p = 0$ and hence $q = 3.5$. In the numerical experiment shown in Fig. 3, we adopt a constant strength of $Q^* = 10^8 \text{ ergs/g}$, and initialize the particle size distribution with $dn/ds \propto s^{-4}$. We ignore collisional cooling here by restricting bodies to only one eccentricity bin ($e = 0.15$). Irrespective of the power-law we choose for the debris redistribution, we find that small bodies in the system settle into the expected $q = 3.5$ form and larger bodies gradually enter into collisional equilibrium as time goes on.

If the collision energy is too low to cause destruction,

we separate the outcomes into two further categories: rebound or conglomeration. In our code, conglomeration occurs when the relative velocity falls below ten times the mutual escape velocity. This disfavors conglomeration of small bodies: kilometer-sized bodies only accrete each other when $e \lesssim 10^{-3}$ at Kuiper belt distances.

When this is not satisfied, the bodies rebound, with both having the same e ($=e_f$, Eq. 7). We do not model either cratering collision or sticking by chemical forces. In the following, we discuss in more detail the accretion process.

2.4. Collisions: accretion

The collisional cross sections in eq. (6) lead to the following rates of accretional growth (GLS), for bodies with size R and velocity dispersion u , accreting smaller bodies of surface density σ and velocity dispersion u (with $u > v$)

$$\frac{1}{R} \frac{dR}{dt} \sim \frac{\sigma\Omega}{\rho R} \alpha^{-1} \begin{cases} \left(\frac{v_H}{u}\right)^2, & v_H < u < v_{\text{esc}}, \\ \left(\frac{v_H}{u}\right), & \alpha^{\frac{1}{2}} v_H < u < v_H, \\ \alpha^{-\frac{1}{2}}, & u < \alpha^{\frac{1}{2}} v_H. \end{cases} \quad (11)$$

We confirm that our numerical algorithm does reproduce the above relations. There is a subtlety here. These expressions assume an isotropic velocity dispersion, $i \approx e$. However, when stirring is in the sub-hill regime ($u < v_H$, eq. 2), inclinations of bodies are excited at a lower rate than their eccentricities, while both quantities are damped by dynamical friction at comparable rates. We then expect these bodies to satisfy $i \ll e$ and the accretion rate should proceed as the super-thin case (GLS), in which case the accretion rate is $\sigma\Omega/(\rho R) \cdot \alpha^{-3/2}$ for all $u < v_H$. In practice, however, stirring is contributed by bodies of various sizes, not just the largest sizes. Short of tracking the inclination evolution, it is difficult to ascertain the accretion geometry. So in this work, we simply assume an isotropic velocity dispersion even though it carries mistakes that may reduce accretion rate by up to $\alpha^{-1/2}(u/v_H)$. This, as it turns out, is more significant when dealing with accretion among big bodies.

Here we comment on another numerical detail concerning the growth of the largest bodies. When two bodies (m_1, m_2 , with $m_1 < m_2$) merge, the combined mass in the new body typically falls between m_2 and the next mass bin (m_3). We deposit two fractional bodies in the m_2 and m_3 bins, respectively, requiring that the total mass be $m_1 + m_2$ and the total particle number be 1. This causes no major concern except where the fractional body in m_3 (number count n_3) is the largest body in the system and it accretes much more quickly than other bodies. We then have a fractional body running away from the pack. To avoid this unphysical outcome, we adopt a so-called ‘large body gating’ procedure, which effectively allows the fractional body in m_3 to advance to the next mass bin (m_4) only when the total mass in this bin has grown by $n_3(m_4 - m_3)$. In such a gating procedure, promotion occurs when the number of the largest body has reached at least unity. It emulates the growth speed of an individual large body, preventing inordinate run-away. Testing shows that this method reproduces the large body growth rates as in Goldreich et al. (2004b). In reality, there is usually a single most mas-

sive body in each accretion zone. Our approach here effectively assumes that the size of our simulation box is the size of the accretion zone. The validity of such a crude numerical approach should be verified with codes that incorporate N-body dynamics to reach beyond the statistical approach.

3. CONGLOMERATION: RESULTS AND ANALYSIS

In the remainder of this paper, we present the results of a number of *collisionless* simulations, in which rebounding and destructive collisions are disabled in the code, but conglomeration still occurs when bodies collide at a speed less than ten times their mutual escape speed. We focus on collisionless simulations in order to compare with previously published results, in which typically small bodies collide less than a few times over the course of the simulation. In an upcoming paper, we shall consider the effects of collisional damping and destruction.

We present detailed results from a fiducial simulation in Fig. 4, with Figs. 5 - 6 providing diagnostic details. For ease of comparison, we initialize our planetesimal disk similarly to those in previous works (Kenyon & Luu 1998, SS11). Our disk is made up of $s = 1$ km planetesimals with a surface density of $\sigma = 0.1 \text{ g/cm}^2$, comparable to the solid value in a MMSN disk. Spread over a radial width of $\Delta a/a = 0.13$ at $a = 45$ AU, this corresponds to a total mass of $10M_\oplus$. The bodies ($\sim 10^{13}$ of them) are initially placed on dynamically cold orbits with $e = 10^{-7}$.

The growth of the largest bodies is mainly due to accretion of kilometer bodies, at all times. So an important quantity to focus on is eccentricity of the km bodies. The following scalings for the Kuiper belt region will prove useful: $e_{\text{esc}} = v_{\text{esc}}/v_{\text{kep}} \sim 10^{-1}(R/10^8 \text{ cm})$, where v_{esc} is the escape speed from a body of size R , and $e_H = v_H/v_{\text{kep}} \sim \alpha^{1/2} e_{\text{esc}} \sim 10^{-3}(R/10^8 \text{ cm})$. We also discuss two related distributions: the number distribution and the mass distribution. If the number distribution is $dn/dR \propto R^{-q}$, then the mass distribution is $dm/d \log R \propto R^{4-q}$.

The km bodies have a mean collision frequency

$$\nu = \frac{\sigma\Omega}{\rho s} \sim 10^{-7} \text{ yr}^{-1}. \quad (12)$$

This is the natural timescale in the problem of interest. So from now on, we express time always in unit of $t\nu$.

3.1. Three Growth Stages

The growth can be naturally divided into a few stages.

1. Geometric accretion Initially, stirring is much faster than growth until $e \sim e_{\text{esc}}$, and hence the initial growth is dominated by pair-wise conglomeration among equal-sized bodies (size s). Assume collisions occur with geometric cross-section. At time $t\nu \ll 1$, the average collision probability for each of the 10^{13} km-sized bodies is $(t\nu)$, but the probability of a single body having experienced N collisions is $(t\nu)^N$. The size distribution at this point falls off steeply with R . The largest body possible at time t is determined by $(t\nu)^N 10^{13} = 1$, or at a radius of

$$R_{\text{max}} \approx \left[\frac{-\log(10^{13})}{\log(t\nu)} \right]^{1/3} s. \quad (13)$$

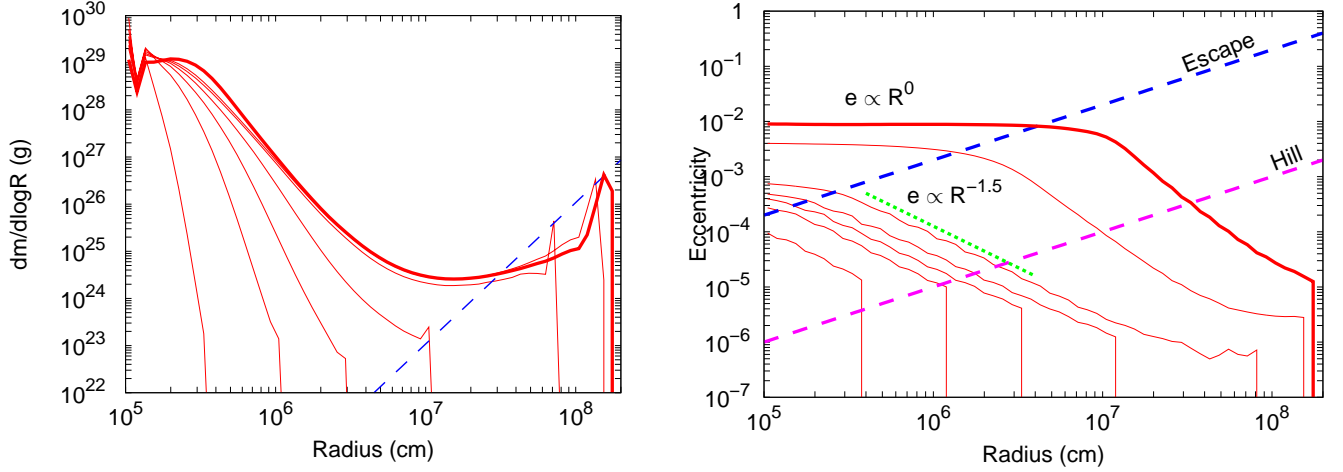


FIG. 4.— Results from our fiducial simulation of collisionless conglomeration, starting from a disk of 1 km bodies with a surface density $\sigma = 0.1 \text{ g/cm}^2$, and an initial eccentricity of $e = 10^{-7}$. The left panel shows the evolution of differential mass and the right panel eccentricity, plotted as functions of body sizes. Data are taken at 0.2, 4, 8, 12, 16, 20 (all thin lines) and 40 Myrs (thick line), corresponding to $t\nu = 0.02, 0.4, 0.8, 1.2, 1.6, 2.0$ and 4. In the left panel, the dashed line indicates 1 body per mass bin, and the upturn in differential mass at the largest size bin is caused by the requirement that there be at least one full body in the most massive bin, as modelled by our ‘large-body-gating’ procedure (see §2.4). At 40 Myrs, the number distribution of large bodies (100–1000 km, disregarding the upturn) can be roughly described by a power-law, $dn/dR \propto R^{-q}$ with $q \sim 4$. The efficiency of conglomeration, defined here as the mass fraction above 100 km, is 10^{-3} . On the right panel, the two dashed lines correspond to the surface escape velocity and Hill velocity from bodies of that size. At 40 Myrs, small bodies are uniformly stirred by the largest bodies ($e \propto R^0$), while larger bodies experience dynamical friction from the seed planetesimals.

So at $t\nu \sim 0.3$, the largest body has a size of $R \sim 3 \text{ km}$ (ignoring gravitational focusing; see below). By this time, km bodies have stirred each other to $\sim 1/2$ of their escape velocities (eq. 2), or, $e \sim 10^{-4}$, much above e_H of the largest bodies already formed.

2. Rapid Run-away If small bodies are super-hill, the largest bodies experience run-away. They pull away from the rest of the pack while carrying little total mass (left panel of Fig. 4). Eq. (11) indicates that the slowest growth occurs at the smallest size. So once the geometric accretion produces bodies with $R \sim 3 \times s$, the bottle-neck is overcome and very large bodies can be conglomerated within a comparable amount of time.

During this stage of rapid runaway, the small bodies dominate the stirring, and their eccentricities increase very gradually (see Figure 5). The big bodies grow faster than they can stir, and their size spectrum is very steep, $q \gg 4$. With time, u/v_H decreases towards unity and we enter the following newly-discovered phase of growth (Lithwick 2013).

3. Trans-hill growth (or slow run-away) Rapid run-away ends once the big bodies dominate the stirring. Thereafter, the big bodies’ stirring interferes with their feeding, and the big bodies grow at the same rate as the small bodies’ eccentricities are stirred. Equating the two yields

$$\frac{\Sigma}{\sigma} \alpha^{-1} \left(\frac{v_H}{u} \right)^2 \approx 1. \quad (14)$$

For our simulation, this is satisfied when $R_{\text{max}} \sim 100 \text{ km}$, with small body $e \sim 10^{-4}$, and $\Sigma/\sigma \sim \alpha \sim 10^{-4}$, at a time of $t\nu \sim 1.2$.

The transition point is affected by our treatment of ‘large body gating’. If one employs a more stringent ad-

vance criterion than what we adopt, for instance, the mass density Σ at a given size will be greater as the run-away (which thins out the number) is more restrained. So the transition would occur at a smaller R . This transition point is also affected by the value of u . If the initial excitation is $e = 10^{-3}$, for instance, the transition would occur at $R = 10^3 \text{ km}$ with again $\Sigma/\sigma = 10^{-4}$. Lastly, this transition point is affected by the initial size spectrum of big bodies.

Let us define a class of trans-hill bodies ($R_{\text{trans}}(t)$) which always satisfy $v_H \approx u(t)$. These bodies are $\sim 100 \text{ km}$ when the rapid run-away transitions to slow run-away. Following Lithwick (2013), we argue that these trans-hill bodies remain effectively the main stirrers in the system, $R_{\text{stir}} \approx R_{\text{trans}}$, or equivalently, $u \sim v_H(R_{\text{stir}})$, in subsequent growth. Hence the name ‘trans-hill’ growth.

To demonstrate this must be true (for a more detailed explanation, see Lithwick 2013), we consider the growth of bodies above and below $R_{\text{trans}}(t)$. Growth of bodies with $R < R_{\text{trans}}$ is in the super-hill (runaway) regime. Their growth rate (eq. 11) can be written as

$$\frac{1}{R} \frac{dR}{d(t\nu)} \approx \frac{s}{R_{\text{trans}}} \alpha^{-1} \times \frac{R}{R_{\text{trans}}} \quad (15)$$

Since this decreases with decreasing R , the size spectrum for $R < R_{\text{trans}}$ is largely frozen.

Growth of bodies with $R > R_{\text{trans}}$ is in the sub-Hill (orderly) regime. The shape of their size spectrum remains invariant with time. Since the initial size spectrum falls steeply beyond $R > R_{\text{trans}}$, stirring is initially dominated by bodies of size R_{trans} . And this will remain so throughout the trans-hill growth.

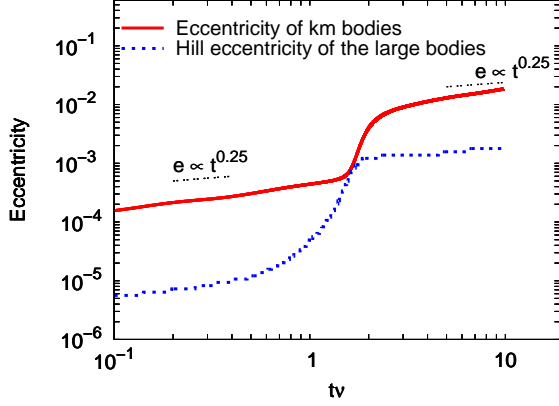


FIG. 5.— Evolution of the eccentricity of km planetesimals is plotted here against the dimensionless time (solid red curve), for the simulation presented in Fig. 4. The Hill eccentricity of the largest bodies at any given time, $e_H(R_{\max})$, is plotted as a blue dashed curve. In the geometric accretion phase ($tv < 0.3$), the small bodies self-stir to produce $e \propto t^{1/4}$. Rapid run-away follows once the growth bottle-neck is overcome. In this phase, e remains roughly constant as stirring is dominated by the inefficient small bodies, while e_H rises steeply. After $tv \sim 1.2$, the growth of the big bodies is hampered by their own stirring, and the largest bodies remain trans-hill during growth, $e \sim 2.5e_H$. After $tv \sim$ a few, growth effectively stalls and e is again stirred up gradually as $e \propto t^{1/4}$. See text for more details.

As a result of these two considerations, $u \approx v_H(R_{\text{stir}})$ during the trans-hill growth. Equation (14) continues to hold, so the size spectrum extends to larger and larger sizes with $\Sigma \sim \text{const}$, or $q \approx 4$. This is the value we find in our simulations,² and is similar to the results of Kenyon & Luu (1998), Ormel et al. (2010), and SS11. An explanation for the slope of the size spectrum, different from our above one, is given in SS11. We discuss our different interpretations further in §4.

In our simulations, bodies as large as 1000 km are formed by $tv \sim 2$. This is consistent with the mass-doubling time for the stirring bodies one obtains from eq. (11), $tv \sim \alpha R/s$.

3.2. End of Growth

The efficiency of formation, defined here as the mass fraction in bodies larger than 100 km, reaches $\sim 10^{-3}$ towards the end of trans-hill growth (Fig. 6). The largest bodies formed are ~ 1000 km, or Pluto-sized. We argue below that the growth effectively stops when these values are reached. In other words, collisionless conglomeration produces large bodies but at a very low efficiency.

During slow run-away, equation (14) is continuously satisfied, yielding $\Sigma/\sigma \sim \alpha$. So the largest size bodies that can form in our simulation, insisting on at least one such body, is ~ 1000 km (see the line in Fig. 4 that represents each bin containing one single body). And

² The mass distribution shown in Fig. 4 shows a departure from $q = 4$ for the largest bodies. This is a consequence of the fact that our numerical procedure insists on at least one single most massive body (‘large body gating’).

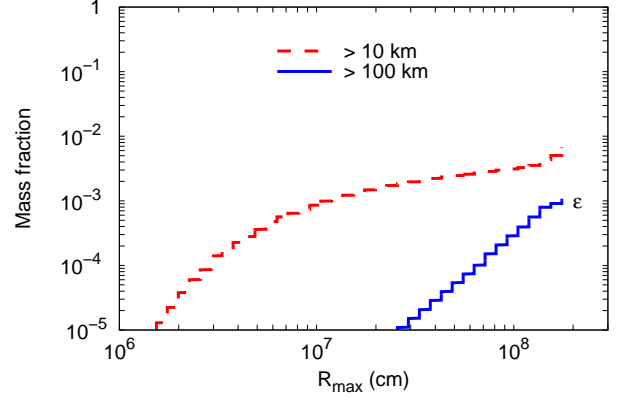


FIG. 6.— Fractions of initial mass that are incorporated into large bodies (solid for bodies with $R > 100$ km and dashed for $R > 10$ km, as a function of R_{\max} (also the most effective stirrer, R_{stir}). In the text, we define the efficiency of formation, ϵ , as the mass fraction above 100 km, with $\epsilon \sim 10^{-3}$ towards the end of the simulation.

indeed we observe that evolution practically stalls when $R_{\max} \approx 1000$ km. The formation efficiency, defined as the fractional mass accumulated in bodies greater than 100 km, is then

$$\epsilon = \frac{1}{\sigma} \int_{100 \text{ km}}^{R_{\max}} \Sigma d \log R \approx \text{a few } \alpha, \quad (16)$$

and is of order 10^{-3} in the Kuiper belt region. In Lithwick (2013), we argue that trans-hill growth is typically terminated when a single big body dominates its own feeding zone, i.e., when the biggest bodies become oligarchs (Kokubo & Ida 1998).

Our statistical code loses validity once the oligarchic phase commences. A statistical code coupled with N-body dynamics is needed. However, we can project the subsequent growth fairly robustly for the Kuiper belt region, since oligarchy likely did not play an important role there.

After trans-hill growth is terminated, small bodies are stirred to super-hill velocities, as $u \sim t^{1/4}$ until u reaches $v_{\text{esc}}(R_{\max})$ (Fig. 5). With such a hot population of small bodies, accretion by the big bodies proceeds with geometrical cross-section. Yet geometric accretion is far too inefficient to form the observed population of Kuiper belt objects within the Solar system lifetime.³ So there is no subsequent accretion to raise the efficiency of big body formation much above $\sim 10^{-3}$. This low formation efficiency is a consequence of our neglect of collisions amongst small bodies. In a forthcoming paper, we show that when collisions are included, the formation efficiency can rise to nearly 100%.

Growth is likely to evolve into the collisional regime. Even if planetesimals start as km-sized, as they are continuously stirred, they approach their destruction speed at $e \sim 10^{-3}$ (eq. 9). Their mutual collisions beyond this point should be destructive and will produce many small debris. When this occurs, collisional cooling among small

³ Pluto, for instance, has a geometrical optical depth of $(1000 \text{ km}/40 \text{ AU})^2 \sim 10^{-14}$.

planetimals can no longer be ignored. Growth will then be in the collisional limit.

A minor caveat concerns our assumption of isotropic velocity dispersion for all bodies. For large bodies which stir each other in the sub-hill range, the inclination dispersion may fall much below that of their eccentricities (Rafikov 2003; Goldreich et al. 2004b). It is likely that accretion among large bodies could proceed then at a rate greater than that adopted here.

3.3. Simulations with Different Initial Conditions

Our above understanding of the conglomeration process allows us to explain the following dependences when initial conditions in the simulation are altered. In all cases, we find a similar size spectrum to that obtained above. We delay the discussion on the α -dependence to §4.1.

- **initial eccentricity** We compare the growth of bodies with initial eccentricities ranging from 10^{-7} to 10^{-3} , with all other properties held constant. The escape velocity from km bodies is $e \sim 10^{-4}$ at 45 AU. We find that simulations with initial velocity dispersion smaller than this quickly converge to our standard case; while those with velocity dispersion above this value first undergo orderly growth and produce a more significant mass in intermediate class bodies. In all case, the final efficiency is $\epsilon \approx 10^{-3}$.
- **initial surface density** We vary the initial surface density of solids from 10^{-3} times to 10 times the MMSN values (our standard case being 1 MMSN), with an initial eccentricity of $e = 10^{-7}$. We observe that the growth time scales inversely with the surface density (Fig. 7). This is because the natural timescale in the problem is the small body collision time (eq. 12). This result has been reported by Kenyon & Luu (1998). We also find that higher mass disks can harbor larger R_{\max} – the final size of the largest body scales roughly as $\sigma^{1/3}$, a result of us insisting that the largest bin has at least one whole body. Lastly, the efficiency of formation only depends logarithmically on the initial σ .
- **seed size** We perform a suite of simulations with different starting sizes ranging from 10 m to 10 km. Since the mean collision time (eq. (12)) scales inversely with starting size, and the entire evolution takes place within a few collision times, we expect that a smaller starting size leads to quicker growth. This is observed in Fig. 8 where the growth time scales roughly as $\nu^{-1} \sim 10^7(s/1km) \text{ yrs.}$ ⁴ The size of the largest bodies that form and the size spectrum are comparable in all simulations. More importantly, the efficiency of formation (ϵ) remains similarly low in all cases.

To summarize, changes in surface density and seed size primarily affect the conglomeration results through their effect on the mean collision frequency (eq. 12).

⁴ This is steeper than the relation of $s^{1/3}$ found by Kenyon & Luu (1998). We suspect that this may relate to their initial conditions of super-escape velocity dispersions.

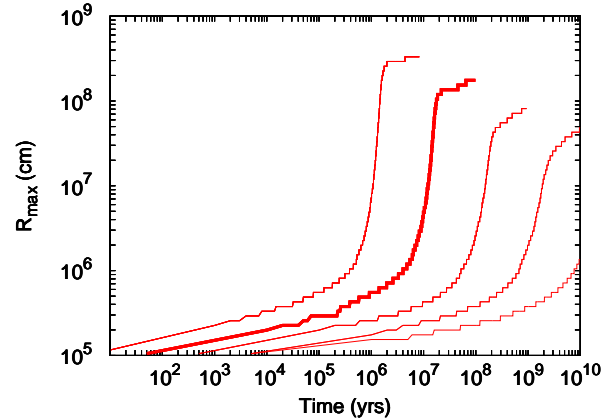


FIG. 7.—: Growth of R_{\max} as a functions of time, for disks with different surface densities. The total mass spans from 10^{-3} MMSN (bottom-most curve) to 10^{-2} , 10^{-1} , 1 and 10 MMSN (top-most curve), with the thick red curve being our fiducial case (Fig. 4). We find the timescale of runaway growth obeys $t \propto \sigma^{-1}$. All growth follow the pattern of a rapid run-away, followed by a slow run-away, and ending when the largest bin contains only one body.

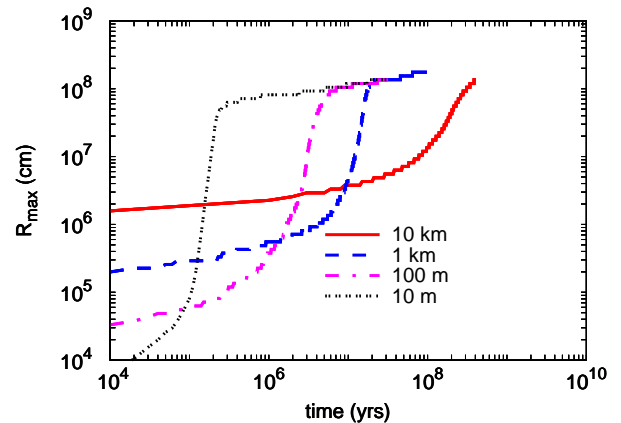


FIG. 8.—: Growth of the largest body in simulations with different seed sizes. Bodies grow slowly at first, with the velocity dispersion set by the escape velocity of the seed bodies. Eventually a few bodies run away, when they are sufficiently large. The timescale of runaway increases linearly with starting size. However, the largest bodies that formed are similar in size.

4. COMPARISON WITH PREVIOUS WORKS

4.1. SS11

While earlier works (Kenyon & Luu 1998; Kenyon & Bromley 2008; Ormel et al. 2010) have performed exhaustive studies of the conglomeration process, SS11 is the first to present a simple analytical argument for the numerical results. Here, we critically examine their argument.

SS11 aims to explain the $q = 4$ spectrum, obtained by all works, as a result of equal accretion. They assume that the largest bodies grow by accreting each other and by accreting small bodies at equal rates (‘equal accre-

tion’). This assumption, which was not properly justified or numerically confirmed in their study, enables them to derive the mass spectrum. They find $q = 4$, with a (constant) efficiency of large body formation of $\epsilon \sim \alpha^{3/4}$. These claims appear to be backed up by their simple yet elegant numerical experiments.

However, it is unclear why, on physical grounds, equal accretion should occur. Instead, we have shown that the $q = 4$ spectrum arises due to the fact that the largest bodies at any given time are trans-hill relative to the small bodies. We present a physical argument why this is naturally achieved (§3.1). As is shown explicitly in Fig. 9, we do not find accretion among large bodies to be important (also see Lithwick 2013). Our expected efficiency of growth is $\sim \alpha$ (see Fig. 12). The difference between this and SS11’s efficiency of $\alpha^{3/4}$ is less easy to discern numerically since the two predictions differ by a very weak power of α .

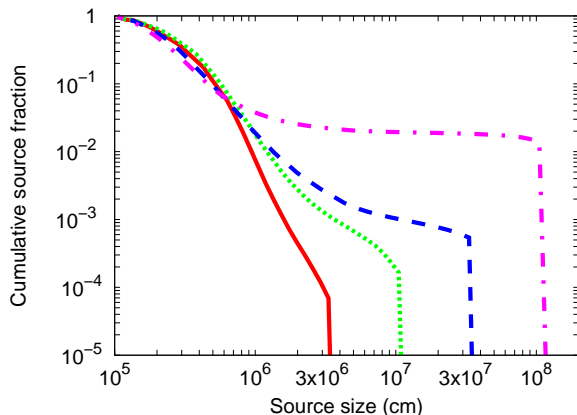


FIG. 9.—: Cumulative contribution (by mass) to the accretional growth of R_{\max} -sized bodies from bodies of various sizes, for the simulation shown in Fig. 4, when $R_{\max} = 30, 100, 300$ and 1000 km. Accretion of small bodies always dominates the growth, with contribution from bodies of similar sizes reaching at best a few percent of the total accretion. This is in contrast to the ‘equal accretion’ assumption in SS11.

For a closer comparison, we have written a simplified code to emulate the SS11 simulations. We adopt their set of initial parameters ($40M_{\oplus}$ in 1 km objects orbiting at $35 - 45$ AU with $e = 3 \times 10^{-6}$), and their simplifications whereby bodies feel dynamical friction from smaller bodies; bodies are viscously stirred only by bodies bigger than or equal to themselves; and all collisions lead to accretion. We also adopt analytical dynamical friction and viscous stirring rates (equations 2-3, 11). For the collision rate, we adopt Equation (11).⁵

⁵ Our collision rate differs slightly from SS11 in the sub-hill regime, in that we assume accreted bodies have isotropic velocity dispersion (Eq. 11) whereas SS11 assume they are super-thin. This difference is unlikely to be important because in both our and their simulations the small bodies have $u \gtrsim v_H$, while the biggest bodies are sufficiently dynamically cold ($v \lesssim \alpha^{1/2} v_H$) that the two rates are the same. Although we attempted to follow the exact prescription of SS11, the sharp discontinuity in accretion rate at

We compare results of our simulation to that of SS11 in Fig. 10 and find good agreement in the formation efficiency and the size spectrum. One difference, however, is that we find a drastically shorter timescale for growth in our simulations, by almost a factor of 100 compared to that in SS11.⁶ The results of this simplified simulation also qualitatively agree with those of our full coagulation simulation shown in Figure 4—in particular, the size spectrum and efficiency at late times are comparable. However, there are a number of differences in the details, which are partly due to the neglect of viscous stirring by smaller bodies in the SS11-type simulations.

Focusing on the issue of equal accretion, Fig. 11 shows that even in a simulation that is tuned to closely match SS11, and that largely reproduces their results, accretion of small bodies dominates the growth. We do observe that accretion of big bodies stays at a constant fraction of the total growth ($\sim 10\%$), as is the case for trans-hill growth (see Section 5.1 of Lithwick 2013). If we were to adopt the superthin accretion formula in our simulations, it is likely that this fraction would be closer to equal accretion. But the fact that our simulations produce $q \approx 4$ shows that equal accretion is not a necessary ingredient for forming the size spectrum.

Lastly, we address the issue of formation efficiency. While SS11 predicted that the final conglomeration efficiency should scale as $\alpha^{3/4}$, we predict $\epsilon \sim \text{a few} \times \alpha$. In Fig. 12, we explore a range of α from 10^{-2} to 10^{-5} , corresponding to a heliocentric distance from 0.4 to 400 AU. We use the simplified code (rather than our full code) and find that our predicted scaling provides a good fit to the numerical results, though we cannot exclude the SS11 scaling due to the small numerical range.

4.2. Kenyon & Luu (1998)

We conduct a second comparison, to the simulations of Kenyon & Luu (1998). We choose this paper for comparison over subsequent ones from the same group because simulations in this paper experiences negligible influence from the gas dynamics and have initial conditions that are the closest to our set-up. They begin with bodies of a single size (we will compare here to their 800 m case), with a total mass of $10M_{\oplus}$ in an annulus from 32 to 38 AU and an eccentricity of $e = 10^{-3}$. This value corresponds to the escape velocity from 10 km-sized bodies. So the early accretion (before reaching 10 km) proceeds slowly without the benefit of gravitational focussing. Adopting their initial parameters, our conglomeration code yields size of the largest body at any given time, $R_{\max}(t)$, as in Figure 13. The growth time in our simulations agree within $\sim 30\%$ from those in Kenyon & Luu (1998).

One significant difference appears when we compare the size distributions. Kenyon & Luu (1998) report a quantity r_5 (defined by the cumulative number $n(> r_5) =$

$v \sim v_H$ for the superthin formula led to severe difficulties with the simulations.

⁶ This difference in timescales is puzzling. But we note that when small bodies have $u \sim v_H$, as they do in our simulations, the timescale to grow bodies of size R is $t \sim R\rho\alpha/(\sigma\Omega) \sim 10^5 \text{ yr} \times (R/100 \text{ km})$ (Eq. 11), which roughly agrees with the timescale we see in our simulation. In SS11’s simulations, $u \sim 3v_H$, which should lengthen the accretion time by the factor $(u/v_H)^2 \sim 10$, not 100.

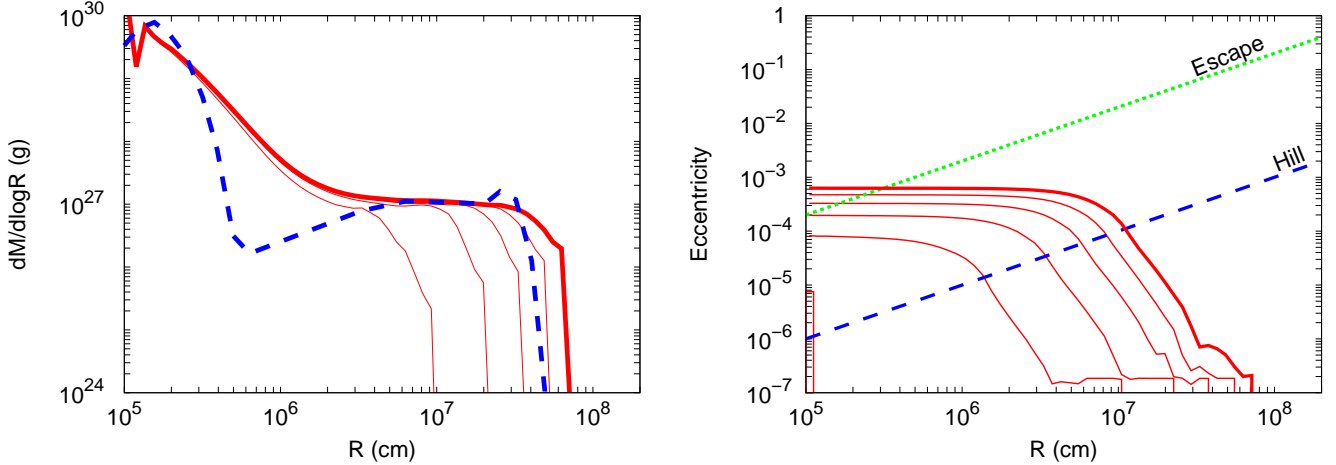


FIG. 10.— Similar to Fig. 4, but for a simulation that is tuned to closely match that of SS11. Results are plotted every 10^5 yrs, ending at 5×10^5 yrs. Both the number and size spectrum of large bodies agree roughly with those in SS11 (blue dashed curve in the left panel). The timescales of growth, however, differ substantially.

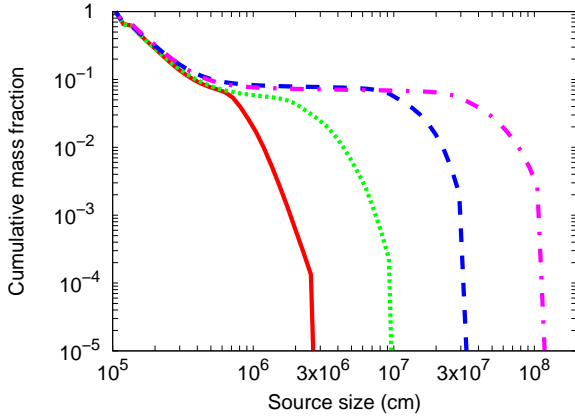


FIG. 11.— Same as Fig. 9, but for a simplified simulation that is tuned to match that of SS11 (see text). Instead of equal accretion of big and small bodies expected by SS11, we observe that accretion from small seeds dominates at all times, with accretion from large bodies staying at a small but constant fraction of the total growth, $\sim 10\%$.

10^5) of 51 km, while we find $r_5 = 31$ km (roughly independent of time at late times). Correspondingly, our formation efficiency ϵ is about 5 – 10 times lower. This difference may be explained by their pseudo-multizone treatment where the big bodies' are prohibited from accreting each other when their respective Hill zones do not overlap. The same effect is observed in Ormel et al. (2010) who also adopt multiple radial zones. We attempt to mimic this effect by imposing a minimum eccentricity floor of 10^{-4} to all bodies (our standard value is 10^{-7}). This keeps the big bodies artificially hot and prevents them from substantially accreting one another. We observe a larger surface density in big bodies and we raise r_5 to 53 km in this case.

5. CONCLUSIONS

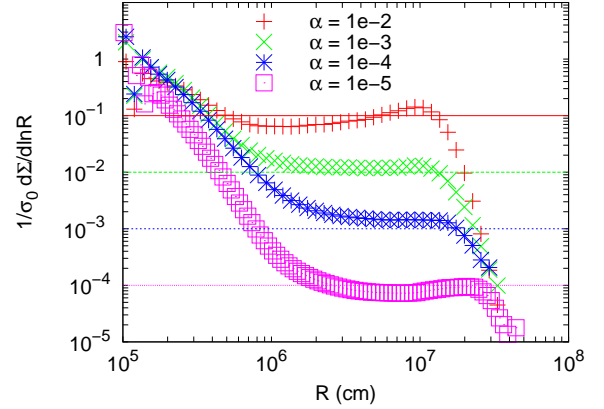


FIG. 12.— The resulting differential mass spectrum from the simplified simulations, for different values of α , where $\alpha = 10^{-4}$ (40AU/a). The efficiency of formation $\epsilon \sim$ a few $\times \alpha$ (the horizontal lines denote 10α for different α value), as predicted by equation (16). This is slightly steeper than the prediction of $\alpha^{3/4}$ by SS11.

In this contribution, we focus on the efficiency of forming large bodies by conglomeration, starting from a sea of small planetesimals that are not cooled by frequent collisions. We find, concurring with previous studies, that the formation efficiency is $\epsilon \sim$ a few $\times \alpha$, or $\sim 10^{-3}$ at the distance of the Kuiper belt.

We obtain this result numerically by constructing a conglomeration code that incorporates physical processes such as viscous stirring, dynamical friction and accretion. This code also has the capability of dealing with catastrophic disruption and collisional damping. But in the current study with seed size of 1 km, collisional cooling is not relevant and we do not allow seeds to break down to smaller particles.

We also derive the formation efficiency analytically (Lithwick 2013). We find that in collisionless environments, growth passes through several stages, but naturally transitions to the most critical stage, which we term

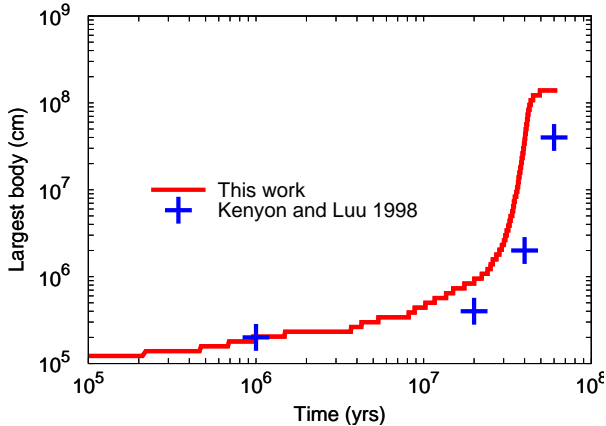


FIG. 13.—: The size of the largest body as a function of time, using our conglomeration code (red curve) and from that of Kenyon & Luu (1998) (blue crosses). The growth rates agree qualitatively, although ours is faster by $\sim 30\%$.

'trans-hill' growth Growth is a run-away process when small bodies are super-hill and an orderly process when small bodies are sub-hill. Consequently, the biggest body at any given time sits at trans-hill, or $u \sim v_H(R_{\max})$. The fact that the system is driven to trans-hill growth is the key for why the size spectrum is $dn/dR \propto R^{-q}$ with $q = 4$, and why the formation efficiency is $\epsilon \sim \text{a few} \times \alpha$.

To be confident of our numerical procedure, we have tested individual components in the code against the order-of-magnitude formulae in GLS. We have also performed detailed comparisons with previous simulations. These include SS11 and Kenyon & Luu (1998). All previous works yield a similarly low formation efficiency, and a similar size spectrum ($q \approx 4$) as we obtain here. But some detailed differences exist. We are able to reproduce the size distribution of SS11 when we follow their numerical procedure, ignoring viscous stirring contributed by small bodies. However, we demonstrate that the key assumption they base their analytical understanding on, that big bodies grow equally by accreting small bodies and by accreting other big bodies, is not what is responsible for the $q = 4$ spectrum and the efficiency. Large bodies grow primarily by accreting small

seeds, and not by accreting each other. Comparison against Kenyon & Luu (1998) show that we reproduce their growth timescale, albeit with a formation efficiency that is five to ten times lower.

In the collisionless limit, trans-hill growth ends when the largest bodies become oligarchs, each responsible for stirring their own food. Subsequent accretion in this phase does not increase significantly the formation efficiency, at least in the Kuiper belt, due to the impossibly long accretion timescale for Pluto-type objects.

Surface densities in large bodies in the Kuiper belt have been measured to be $\sim 10^{-3}$ of that of the MMSN, and the largest bodies are ~ 1000 km in size. These have traditionally been viewed as successes for the collisionless coagulation theory. However, recent discoveries of bright extra-solar debris disks call this into question. Their dust luminosities reveal that they likely harbor large bodies that are a factor of ~ 1000 in number than that in our Kuiper belt (Shannon & Wu 2011), comparable to the total mass in a MMSN solid disk in these outer regions. This conflicts with the low formation efficiency, generic of collisionless conglomeration.

In our simulations, km-size bodies reach such high velocity dispersion towards the end, that their mutual encounter should cause fragmentation into smaller particles. This is also observed in Kenyon & Luu (1999). So even if planetesimals start as large as 1 km, collisional cooling may set in at some stage. An evolutionary path that is qualitatively different from that described here may ensue.

To resolve the issue of long formation timescale for Uranus and Neptune, Goldreich et al. (2004a) have proposed that conglomeration proceeds in a collisional environment, where small bodies are so small they are cooled by frequent collisions. In future works (Shannon et al. 2013a), we follow this path and demonstrate that collisional conglomeration would also be able to raise the efficiency of formation to of order unity, thereby explaining, within one paradigm, the formation of the Kuiper belt and the extra-solar debris disks.

YW acknowledges NSERC and the government of Ontario. YL acknowledges NSF grant AST-1109776.

REFERENCES

- Aumann, H. H., Beichman, C. A., Gillett, F. C., de Jong, T., Houck, J. R., Low, F. J., Neugebauer, G., Walker, R. G., & Wesselius, P. R. 1984, *ApJL*, 278, L23
- Bromley, B. C. & Kenyon, S. J. 2006, *AJ*, 131, 2737
- Brown, M. E., Trujillo, C. A., & Rabinowitz, D. L. 2005, *ApJ*, 635, L97
- Chandrasekhar, S. 1943, *ApJ*, 97, 255
- Collins, B. F. & Sari, R. 2006, *AJ*, 132, 1316
- Collins, B. F., Schlichting, H. E., & Sari, R. 2007, *AJ*, 133, 2389
- Dohnanyi, J. W. 1969, *J. Geophys. Res.*, 74, 2531
- Durda, D. D. & Dermott, S. F. 1997, *Icarus*, 130, 140
- Glaschke, P. 2006, PhD thesis, PhD Thesis, Combined Faculties for the Natural Sciences and for Mathematics of the University of Heidelberg, Germany. XIV+134 pp. (2006)
- Goldreich, P., Lithwick, Y., & Sari, R. 2004a, *ApJ*, 614, 497
- . 2004b, *ARA&A*, 42, 549
- Gomes, R. S., Morbidelli, A., & Levison, H. F. 2004, *Icarus*, 170, 492
- Greenberg, R., Bottke, W. F., Carusi, A., & Valsecchi, G. B. 1991, *Icarus*, 94, 98
- Greenberg, R., Hartmann, W. K., Chapman, C. R., & Wacker, J. F. 1978, *Icarus*, 35, 1
- Hayashi, C. 1981, *Progress of Theoretical Physics Supplement*, 70, 35
- Hornung, P., Pellat, R., & Barge, P. 1985, *Icarus*, 64, 295
- Ida, S. & Makino, J. 1992, *Icarus*, 96, 107
- Jewitt, D. & Luu, J. 1993, *Nature*, 362, 730
- Kenyon, S. J. & Bromley, B. C. 2008, *ApJS*, 179, 451
- Kenyon, S. J. & Luu, J. X. 1998, *AJ*, 115, 2136
- . 1999, *AJ*, 118, 1101
- Kokubo, E. & Ida, S. 1998, *Icarus*, 131, 171
- Krivov, A. V., Sremčević, M., & Spahn, F. 2005, *Icarus*, 174, 105
- Levison, H. F., Morbidelli, A., Vanlaerhoven, C., Gomes, R., & Tsiganis, K. 2008, *Icarus*, 196, 258
- Lithwick, Y. 2013, Submitted to *ApJ*
- Meyer, M. R., Backman, D. E., Weinberger, A. J., & Wyatt, M. C. 2007, in *Protostars and Planets V*, ed. B. Reipurth, D. Jewitt, & K. Keil, 573–588
- Nishida, S. 1983, *Progress of Theoretical Physics*, 70, 93
- Ohtsuki, K., Stewart, G. R., & Ida, S. 2002, *Icarus*, 155, 436

- Ormel, C. W., Dullemond, C. P., & Spaans, M. 2010, *Icarus*, 210, 507
- Parker, A. H. & Kavelaars, J. J. 2012, *ApJ*, 744, 139
- Parker, A. H., Kavelaars, J. J., Petit, J.-M., Jones, L., Gladman, B., & Parker, J. 2011, *ApJ*, 743, 1
- Rafikov, R. R. 2003, *AJ*, 126, 2529
- Safronov, V. S. 1969, *Evoliutsiia doplanetnogo oblaka.*, ed. Safronov, V. S.
- Schlichting, H. E., Ofek, E. O., Wenz, M., Sari, R., Gal-Yam, A., Livio, M., Nelan, E., & Zucker, S. 2009, *Nature*, 462, 895
- Schlichting, H. E. & Sari, R. 2011, *ApJ*, 728, 68
- Shannon, A. & Wu, Y. 2011, *ApJ*, 739, 36
- Shannon, A., Wu, Y., & Lithwick, Y. 2013a, In Preparation
- . 2013b, In Preparation
- Slipher, V. M. & Tombaugh, C. W. 1930, *The Science News-Letter*, 17, 179
- Stern, S. A. 1991, *Icarus*, 90, 271
- Stewart, S. T. & Leinhardt, Z. M. 2009, *ApJ*, 691, L133
- Thébault, P., Augereau, J. C., & Beust, H. 2003, *A&A*, 408, 775
- Thommes, E. W., Duncan, M. J., & Levison, H. F. 1999, *Nature*, 402, 635
- Weidenschilling, S. J. 1977, *Ap&SS*, 51, 153
- Wetherill, G. W. & Stewart, G. R. 1989, *Icarus*, 77, 330
- . 1993, *Icarus*, 106, 190
- Wyatt, M. C. 2008, *ARA&A*, 46, 339